


Article

Design and Test of Duckbill Welding Robot for Cotton Seeder

Yu Ren ^{1,2}, Wensong Guo ^{1,2,*}, Xufeng Wang ^{1,2}, Can Hu ^{1,2} , Long Wang ^{1,2}, Xiaowei He ^{1,2} and Jianfei Xing ^{1,2}

¹ College of Mechanical and Electrical Engineering, Tarim University, Alar 843300, China

² Modern Agricultural Engineering Key Laboratory at Universities of Education Department of Xinjiang Uygur Autonomous Region, Tarim University, Alar 843300, China

* Correspondence: 120120004@taru.edu.cn

Abstract: To improve the automation, welding efficiency, and welding quality of duckbill welding of the cotton seeder, this study designed a cotton seeder duckbill welding robot. According to the characteristics of the duckbill weldment and welding requirements, the overall structure of the welding robot was determined, including the girdle feeding mechanism, static duckbill feeding mechanism, hinge feeding mechanism, welding fixture, welding actuator, and control system. To realize the continuous automatic feeding, positioning, fixing, welding, and unloading of the workpiece in the duckbill welding, the feeding mechanism adopts the method of cooperative cooperation of inductive proximity switch, electromagnet, and cylinder. The main body of the welding fixture adopts the pneumatic clamping method; the welding actuator adopts the synchronous belt module electric drive so that the welding torch can move in a straight line along the X axis and the Z axis. The welding process of the duckbill was simulated by Simufact Welding software, and the deformation and stress changes of the weldment were compared and analyzed when the single-sided single welding, the bilateral symmetrical double welding torch, two welding forms, and two welding process parameters were used to determine the welding process parameters of the welding robot. The prototype was made and the welding test was carried out. The test results show that the duckbill welding robot of the cotton seeder has stable feeding, solid clamping, accurate positioning, and high welding efficiency. According to the national standard, the appearance of the duckbill weld is inspected. The surface of the duckbill weld and the heat-affected zone has no cracks, incomplete fusion, slag inclusion, crater, and porosity. The forming quality of the welded parts is good. The design of the duckbill welding robot for cotton seeder is helpful in solving the problems of cumbersome positioning and clamping and low efficiency in manual and semi-automatic duckbill welding robots, which provides a strong guarantee for the large-scale and standardized welding production of the dibbler duckbill.

Keywords: cotton seeder; duckbill; Simufact Welding; welding robot; automated welding



Citation: Ren, Y.; Guo, W.; Wang, X.; Hu, C.; Wang, L.; He, X.; Xing, J. Design and Test of Duckbill Welding Robot for Cotton Seeder. *Agriculture* **2023**, *13*, 31. <https://doi.org/10.3390/agriculture13010031>

Academic Editors: Jin Yuan, Wei Ji and Qingchun Feng

Received: 21 November 2022

Revised: 9 December 2022

Accepted: 20 December 2022

Published: 22 December 2022



Copyright: © 2022 by the authors. Licensee MDPI, Basel, Switzerland. This article is an open access article distributed under the terms and conditions of the Creative Commons Attribution (CC BY) license (<https://creativecommons.org/licenses/by/4.0/>).

1. Introduction

The plastic mulching technique is one of the most widely used and effective technical measures to improve soil water storage capacity and plant water use efficiency [1,2]. At present, cotton sowing in Xinjiang is based on the method of sowing on film, which is carried out on the soil covered with the film [3,4]. The duckbilled dibbler is used for sowing on film in Xinjiang. The duckbill of the dibbler will cut the film at the sowing position and form holes in the soil. The welding quality of the duckbill of the dibbler is the key to affecting the quality of the hole and the speed of operation [5].

The number of welded duckbills in Xinjiang is about millions every year. Before 2017, the welding method of cotton planter duckbill was manual welding. Welding workers manually position, fix, and weld the three parts of the duckbill, static duckbill, hinge, and girdle. Manual welding has the following problems: unstable welding quality, low efficiency, high labor intensity, and low degree of automation. In 2017, we developed a semi-automatic duckbill welding robot. This semi-automatic welding robot needs to be loaded, positioned, fixed, and unloaded manually, and the welding operation is completed by the

robot. The welding robot improves the welding efficiency of the duckbill. The purpose of this study is to further improve duckbill welding automation, welding efficiency, and welding quality, as well as reduce the labor intensity of welding duckbills.

There are many ways to improve welding efficiency and welding quality. For example, on the one hand, some research can be conducted on harmonic drive transmission [6–8]. This method can improve the welding quality by improving the positioning accuracy of the welding robot manipulator. On the other hand, according to the characteristics of the welding object and the welding requirements, a special welding robot can be designed to replace manual welding [9–13]. For example, Süleyman ERSÖZ et al. [14] proposed a robot system that can automatically complete measurement and welding operations for products that are difficult to manually complete standard measurement or welding operations. Namkug Ku et al. [15] designed a self-driving mobile welding robot for double-hull structures in shipbuilding. Stephen Mulligan et al. [16] developed and demonstrated an autonomous, mobile welding robot capable of fabricating large-scale customized structures. Jiang Yi et al. [17] designed a series-parallel-series hybrid structure mobile welding robot for welding corrugated plates of liquefied natural gas (LNG) membrane tanks. At present, there is little research on the application of special welding robots in the field of duckbill welding of the cotton planters.

Different from the traditional plane welding operation, the weld of the duckbill part is a fillet weld. Its processing technology is complex, the welding workload is large, and the weld is prone to defects [18]. The traditional welding process relies on experience to determine the amount of deformation, the reasonable welding method, and welding process parameters, which rely on experience and cannot fully and quantitatively grasp the law of welding deformation. With the development of finite element technology, the welding simulation is fully applied to the actual production and used to guide the process design and gradually became an effective means to provide technical support for the control of process measures in the welding robot manufacturing process [19–22].

To design a duckbill welding robot to improve the welding quality, stability, and welding efficiency of the duckbill parts of the cotton seeder, this study first analyzes the characteristics of the duckbill parts and then uses Simufact Welding software to simulate and analyze the duckbill welding process, which effectively provides technical support for the welding deformation control process measures of the duckbill welding robot in the manufacturing process. Finally, a cotton seeder duckbill welding robot is designed, and the reliability of the welding robot is verified by the welding test. The research results provide ideas for further improving the quick automatic feeding, clamping, positioning, and welding of the duckbill of the dibbler, as well as provide basic and technical support for the automatic welding of the duckbill of the dibbler.

2. Welding Object Characteristics

2.1. Assembly Structure of Duckbill Welding Parts

The assembly relationship diagram of duckbill welding parts is shown in Figure 1. The dibbler is one of the key components of the cotton mulching seeder, which is used to complete the seeding process. Sowing quality has a significant impact on crop growth and yield [23,24]. The duckbill part cuts the film at the seeding position during the seeding operation and forms holes in the soil. The duckbill is welded by three parts: the static duckbill, hinge, and girdle. The welding quality has a very important influence on the hole-forming effect of the dibbler and the seed falling position.

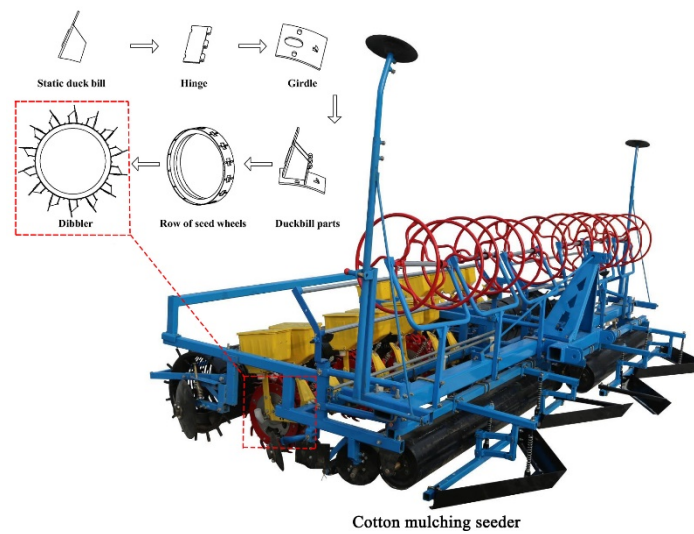


Figure 1. The assembly relationship diagram of duckbill welding parts.

2.2. Material Properties of Duckbill Welding Parts

As shown in Figure 2, the duckbill of a cotton seeder is composed of a girdle, static duckbill, and hinge, and its structural parameters are shown in Table 1. The material of duckbill parts is Q235, which is an ordinary carbon structural steel. The chemical composition and mechanical properties are shown in Table 2. Q235 has low carbon and alloy element content and excellent welding performance. Generally, special process measures, such as preheating and post-weld heat treatment, are not required during welding. However, when the incorrect welding form is adopted, the appearance of the weld will also appear poor, forming cracks.

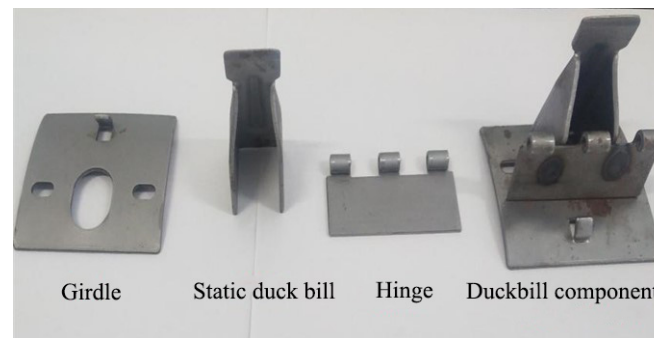


Figure 2. Physical drawing of the duckbill welding parts of the cotton seeder.

Table 1. Structural parameters of duckbill welding parts.

Parts	Length (mm)	Width (mm)	Thickness (mm)	Height (mm)	Mass (g)
Girdle	78.12	68.30	2.11	5.90	73.046
Static duck bill	34.09	27.52	2.57	74.97	77.747
Hinge	69.02	36.11	2.08	7.97	39.281

Table 2. Material properties of Q235.

C (Mass Fraction)/%	Mn	Si	S	P
0.14~0.19	0.30~0.65	0.30	≤0.050	≤0.045
Tensile strength (MPa)		Yield point (MPa)		Elongation (%)
375~500		235		26

2.3. Weld and Welding Requirements Analysis

As shown in Figure 3, the weld of the duckbill welding part is two fillet welds, which are: weld 1 formed by the static duckbill and the hinge and girdle, and weld 2 formed on another back symmetrical surface.

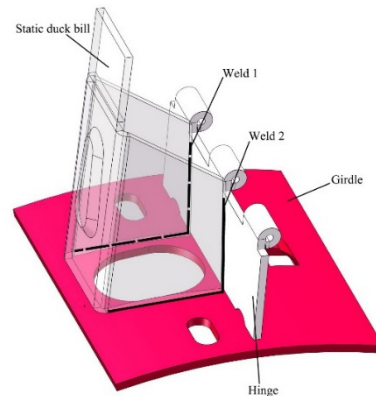


Figure 3. The weld diagram of duckbill welding parts.

An inappropriate welding process will increase the deformation of duckbill welding, resulting in the following problems: (1) the girdle and seeding wheel being difficult to assemble; (2) the following performance being affected; and (3) the quality of the hole being unstable. Duckbill parts in the process of sowing operation need to film soil punching and work under great pressure. The duckbill parts of the welding quality requirements are very high, including the ability to weld duckbill weld surface without cracks, crater shrinkage, and welding tumor defects.

3. Simulation and Analysis of the Welding Process

Welding deformation is the most important factor affecting welding quality. Welding deformation will lead to a manufacturing delay, economic cost, and reduced productivity. Excessive deformation may seriously damage manufacturing in extreme cases, leading to failure [25]. At the same time, high welding residual stresses in the weld can adversely affect the safety and performance of welded components [26,27]. In this study, Simufact Welding software is used to simulate the welding process of duckbill welding parts, and the influence of deformation and the stress of weldments under a single-sided single welding torch and bilateral symmetrical double welding torch, two welding forms, and two welding process parameters, is analyzed.

3.1. Heat Source Model

In welding simulation, a reasonable heat source model is very important for the accurate calculation of post-weld deformation and welding stress [28]. To realize the simulation calculation, the commonly used heat source models are the classical Gaussian distribution heat source model and the double ellipsoid heat source model [29,30]. The Gaussian model can obtain better calculation accuracy for planar high-energy beam welds in simulation calculations. The double ellipsoid heat source model is more close to the actual welding situation of a fillet weld, so this study chooses the double ellipsoid heat source model for calculation.

The heat flux density expression of the front part of the double ellipsoid heat source is:

$$q_f(x, y, z) = \frac{6\sqrt{3}f_t q_0}{abc_f \pi \sqrt{\pi}} \exp\left(-\frac{3x^2}{c_f^2} - \frac{3y^2}{a^2} - \frac{3z^2}{b^2}\right). \quad (1)$$

The heat flux distribution expression of the second half of the double ellipsoid heat source is:

$$q_b(x, y, z) = \frac{6\sqrt{3}f_f q_0}{abc_b \pi \sqrt{\pi}} \exp\left(-\frac{3x^2}{c_b^2} - \frac{3y^2}{a^2} - \frac{3z^2}{b^2}\right). \quad (2)$$

In the formula: a , b , c_f and c_b are oval shape parameters of the heat source; q_0 is the heat input power, and $q_0 = \eta UI$; and f_f, f_b are the heat flux distribution coefficients of the ellipsoid before and after the heat source, $f_f + f_b = 2$.

3.2. Establishment of Welding Model

The solid model of duckbill welded parts was established by SolidWorks, and then the model was imported into Hypermesh for hexahedral meshing. The number of finite element mesh nodes was 37,394, and the number of finite elements was 27,997. The divided model was imported into Simufact Welding for assembly and configuration, as shown in Figure 4. In this study, the weldment material is Q235, and the energy input per unit length of the weld (line energy) is calculated according to Equation (3).

$$Q = \eta \frac{IU}{v} \quad (3)$$

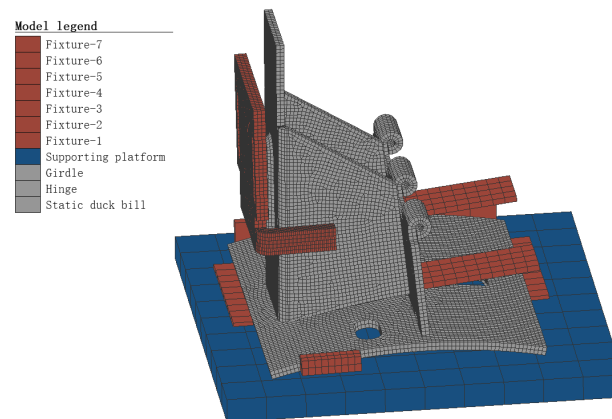


Figure 4. Meshing model of duckbill welding parts.

In the formula: Q is the line energy; I is the welding current; U is the welding voltage; v is the welding speed; and η is the welding thermal efficiency. As the weld of duckbill weldment is fillet weld, the welding heat is relatively concentrated. In this study, the welding thermal efficiency is taken as 0.8 in the simulation process [31].

3.3. Welding Simulation Results and Analysis

3.3.1. Effect of the Unilateral Single Welding Torch and Bilateral Symmetrical Double Welding Torch on Welding Deformation and Stress

Figure 5 shows the deformation of the duckbill welding parts under the single welding torch and the bilateral symmetrical double welding torch. By comparing and analyzing their total displacement cloud diagrams, the following conclusions were obtained: The area of deformation was larger under the condition of the single welding torch. This is because the two sides of the workpiece are uniformly heated and uniformly contracted at the same time by using the bilateral symmetrical double welding torch to reduce the distribution of welding deformation. The maximum displacement difference under the two conditions is 0.09 mm.

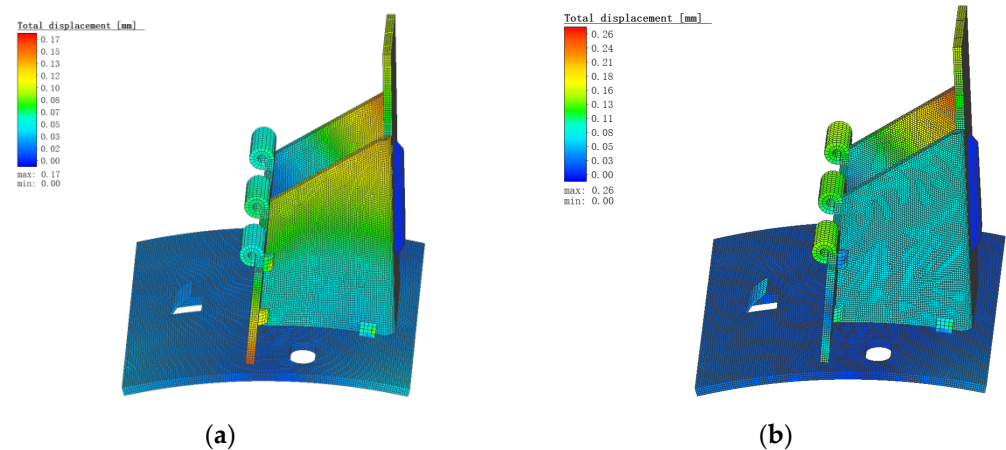


Figure 5. Total displacement diagram of the single welding torch and bilateral symmetrical double welding torch. (a) Single welding torch; (b) bilateral symmetrical double welding torch.

Figure 6 shows the equivalent stress diagram under the condition of the single welding torch and the bilateral symmetrical double welding torch. It can be seen from the figure that under the two conditions, the equivalent stress decreases rapidly from the center of the weld generation area, and then tends to be gentle until it is close to zero. A large stress is generated in the weld zone, which is one of the main reasons for the deformation of the static duckbill. After welding, the weldment is cooling, and the volume shrinkage around the weld is caused by the decrease in temperature. However, the weldment is constrained to prevent its shrinkage, so large tensile stress is generated in the weld area. Under both conditions, the maximum stress difference produced by the duckbill component is 7.28 MPa, but welding a duckbill component with a single torch takes more time than with a bilateral symmetrical double torch. Therefore, this study finally chose the welding method of the bilateral symmetrical double welding torch.

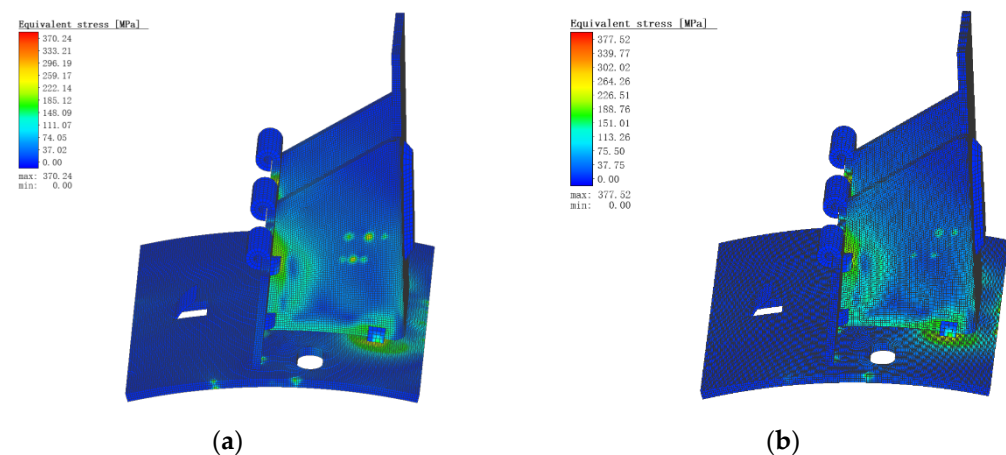


Figure 6. Equivalent stress diagram under the condition of the single welding torch and bilateral symmetrical double welding torch. (a) Single welding torch; (b) bilateral symmetrical double welding torch.

3.3.2. Effect of Welding Form on Welding Deformation and Stress

Figure 7, respectively, shows the use of continuous welding and spot welding under the two forms of total displacement cloud. From Figure 7, it can be seen that the displacement areas of the two were mainly distributed at the top of the static duckbill, and the deformation of the rest was relatively small. This is because the deformation of the fixed part is smaller than that of the free part. The position and deformation of the fixed part will be greatly limited under the action of the clamping device, so the thermal deformation

is reduced during the welding cycle. The maximum displacement of continuous welding is 0.98 mm, and that of spot welding is 0.26 mm. This is because in the weld, continuous welding, compared to spot welding, outputs greater thermal energy.

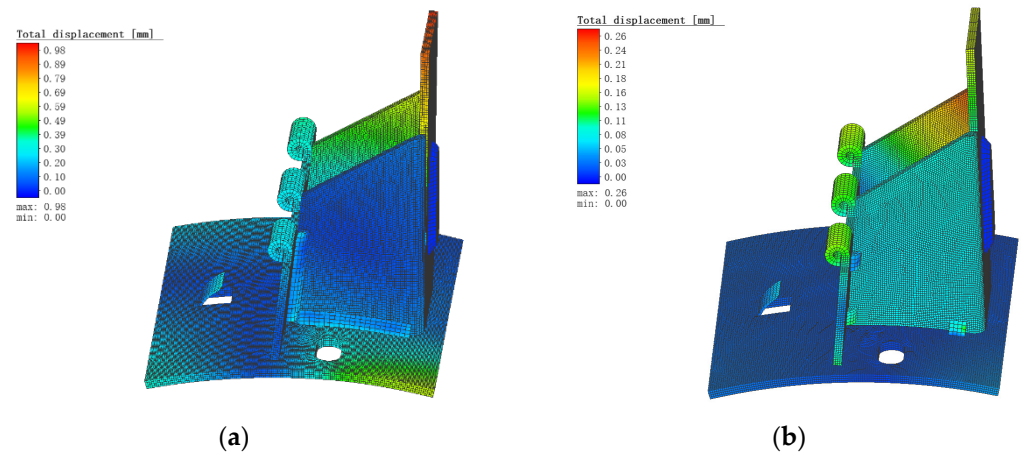


Figure 7. Total displacement diagram under continuous welding and spot welding conditions. (a) Continuous welding; (b) spot welding.

Figure 8 is the equivalent stress diagram of continuous welding and spot welding. It can be seen from Figure 8 that the stress distribution of spot welding is smaller than that of continuous welding, and the difference in their maximum stress value is 121.89 MPa. Their stress distribution is similar, the stress distribution appears to diffuse from the weld to the distance and then weaken, but it is obvious that the stress distribution of continuous welding is wider and wider. This study finally chose the welding form of spot welding.

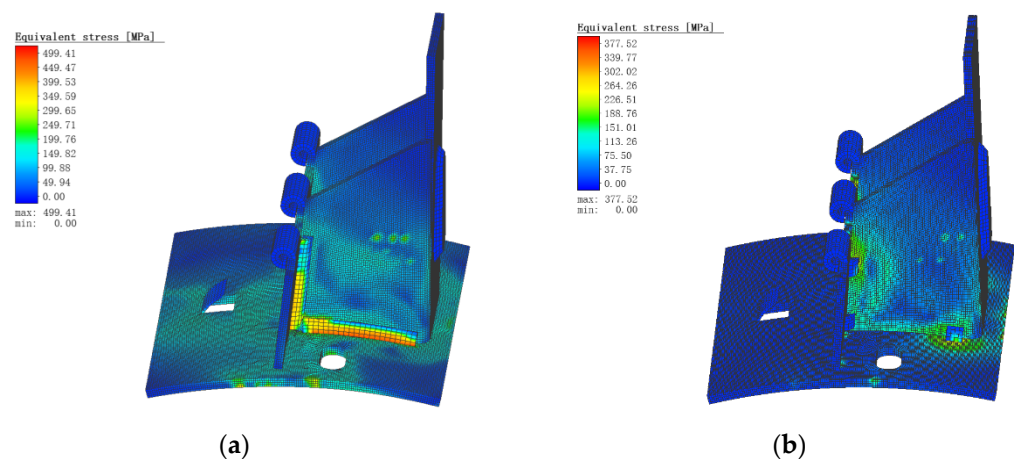


Figure 8. Equivalent stress diagram under continuous welding and spot welding. (a) Continuous welding; (b) spot welding.

3.3.3. Effect of Welding Process Parameters on Welding Deformation and Stress

Figure 9 is the total displacement diagram of the duckbill welded parts when the welding speed is 4 mm/s and 10 mm/s. It can be seen from the figure that the total displacement difference between the two welding speeds is 0.13 mm, but at the welding speed of 4 mm/s, the deformation area is relatively larger. This is because the deposition amount of the wire metal on the unit-length weld is inversely proportional to the welding speed, and the melting width is inversely proportional to the square of the welding speed. Therefore, when the welding speed increases, the energy decreases, the penetration depth and width decrease, and the deformation area is relatively reduced.

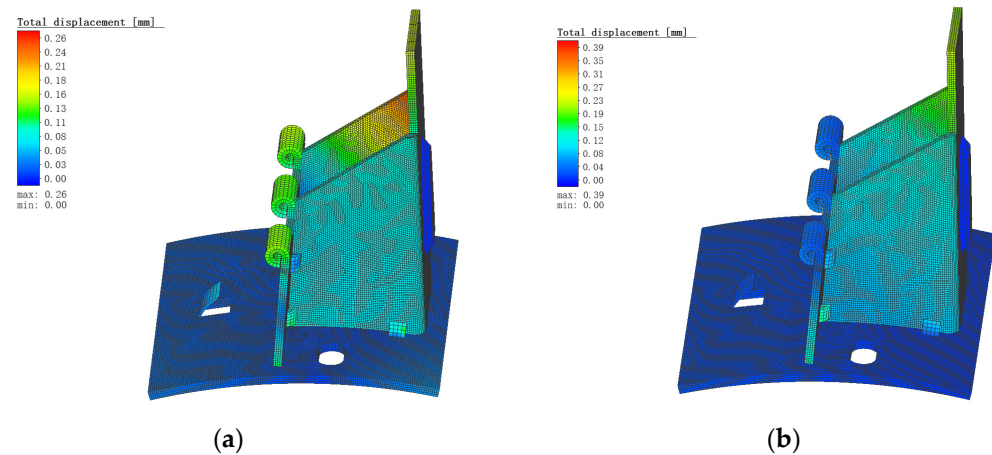


Figure 9. Total displacement diagram at the welding speed of 4 mm/s and 10 mm/s; (a) 4 mm/s; (b) 10 mm/s.

Figure 10 is the equivalent stress diagram under the two welding speeds of 4mm/s and 10 mm/s. As can be seen from the figure: 4 mm/s welding speed under the maximum equivalent stress is larger and the equivalent stress of a wider range of areas. Welding speed is directly related to the size of the welding productivity, and to obtain the maximum welding speed, should be on the premise of quality assurance as far as possible, according to the specific circumstances of the appropriate adjustment of welding speed, to ensure that the weld height and width are the same. In this study, the welding speed is finally selected as 10 mm/s.

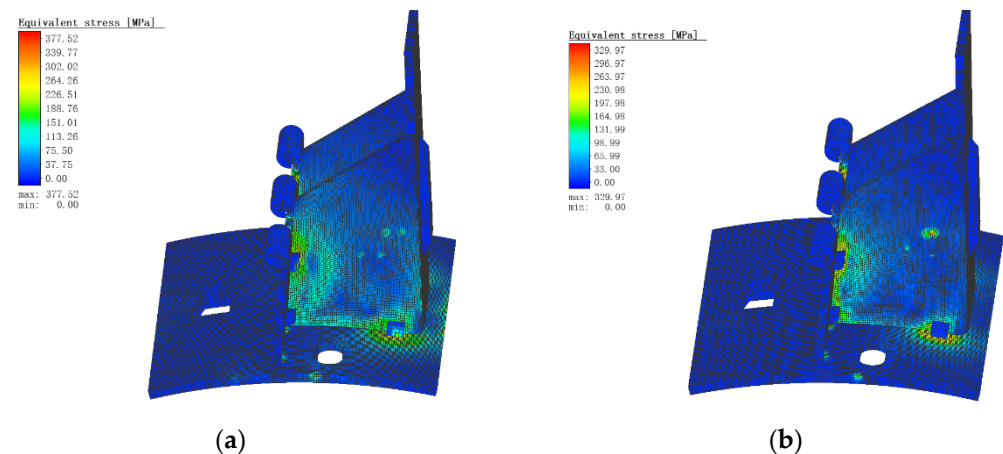


Figure 10. Equivalent stress diagram at the welding speed of 4 mm/s and 10 mm/s; (a) 4 mm/s; (b) 10 mm/s.

4. Design of Duckbill Welding Robot for Cotton Seeder

4.1. Structure Composition and Working Principle

The duckbill welding robot of the cotton planter is mainly composed of a girdle feeding mechanism, static duckbill feeding mechanism, hinge feeding mechanism, support table, welding fixture, welding actuator, and control system, as shown in Figure 11.

Working process: Firstly, the girdle feeding mechanism completes the girdle feeding, and then the hinge and the static duckbill feeding structure completes the feeding work in turn. After the three welding parts of the girdle, the hinge, and the static duckbill are all loaded, the workpiece enters the position to be welded, the clamping cylinder works to clamp the workpiece, and the welding actuator moves and performs welding. After the welding is completed, the welding platform is opened, and the weldment falls to the ground.

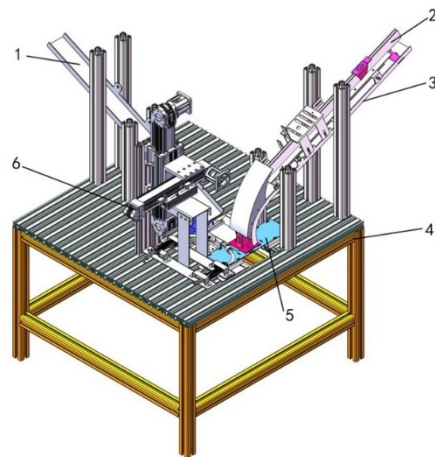


Figure 11. Structure diagram of duckbill welding robot for cotton seeder. 1. Girdle feeding mechanism; 2. static duckbill feeding mechanism; 3. hinge feeding mechanism; 4. support platform; 5. welding fixture; 6. welding actuator.

4.2. Design of Girdle Feeding Mechanism

According to the analysis of the assembly requirements of the duckbill parts, the feeding mechanism needs to meet the following requirements: (1) the hinge and the girdle should be vertical; (2) the static duckbill and the hinge are symmetrically distributed in the transverse center when they are matched with the girdle; (3) the static duckbill should avoid shielding girdle under the mouth. According to the above assembly requirements and the structural parameters of duckbill welding parts, the feeding structure is designed. The feeding mechanism realizes the sequential feeding action of welded parts through the cooperation of an inductive proximity switch, electromagnet, and cylinder.

The structure size of the girdle feeding mechanism is 800 mm × 68 mm × 22 mm. It adopts a modular design and is installed on the support platform through the aluminum profile pillar. The working process is as follows: When the inductive proximity switch detects that there is a girdle in the storage chute, the electromagnet is energized and absorbs the second girdle, and the cylinder shrinks. The first girdle falls freely to the girdle waiting area due to gravity, and finally, the mini cylinder pushes the girdle into the welding area. The girdle feeding mechanism is shown in Figure 12.

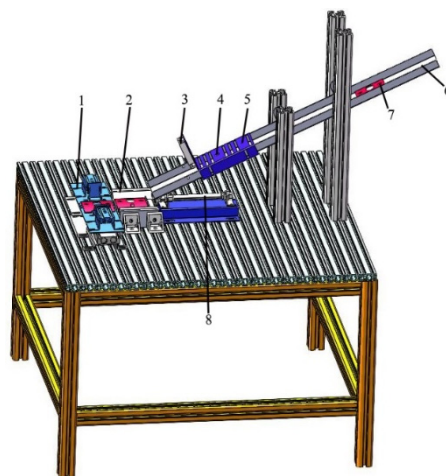


Figure 12. Structure diagram of the girdle feeding mechanism. 1. Welding area; 2. girdle blanking waiting for area; 3. cylinder; 4. inductive proximity switch; 5. electromagnet; 6. storage chute; 7. girdle; 8. mini cylinder.

4.3. Design of Static Duckbill and Hinge Feeding Mechanism

To save space, the static duckbill feeding mechanism and the hinge feeding mechanism adopt an integrated design, and the assembly relationship of the parts is shown in Figure 13. The static duckbill and the hinge feeding mechanism are equipped with fixed plates to fix inductive proximity switches, electromagnets, and cylinders.

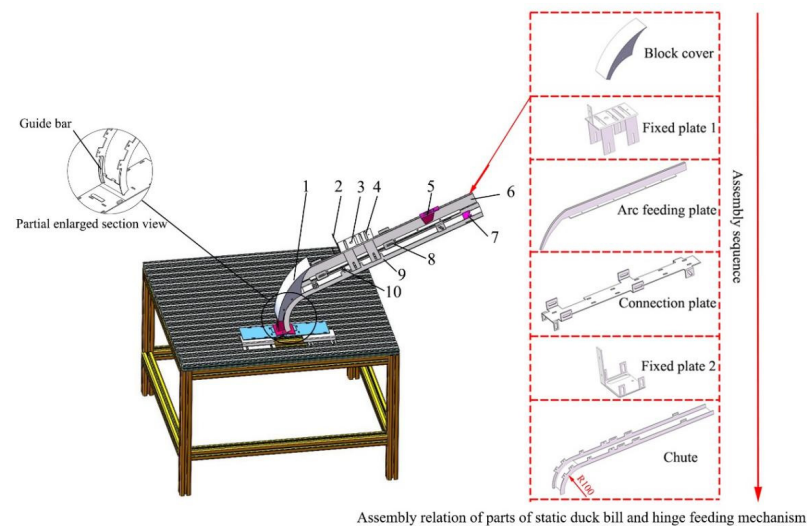


Figure 13. Structure diagram of static duckbill and hinge feeding mechanism. 1. Block cover; 2. cylinder; 3. inductive proximity switch; 4. electromagnet; 5. static duckbill; 6. arc feeding plate; 7. girdle; 8. connecting plate; 9. storage chute; 10. fixed plate 2.

The width of the storage chute of the hinge feeding mechanism is bent according to the dimensions of the hinge, and the bending angle is 90° . To ensure that the hinge is perpendicular to the girdle during blanking, the lower end of the storage chute adopts a circular arc design, and its arc inner diameter is 100 mm. To prevent the hinge from sliding out of the arc guide rail when feeding, the guide bars are symmetrically distributed on both sides to guide and limit displacement. The verticality of the hinge is ensured by limiting the outer side of the guide bar and the arc guide rail. The guide bar is shown in the partially enlarged section view in Figure 13.

The main component of the static duckbill feeding mechanism is an arc feeding plate, and the arc feeding plate is connected with the hinge storage chute through a connecting plate. When the static duckbill is feeding, the contact with the feeding plate is strip contact, and the contact area is small, which greatly reduces the friction when sliding. When sliding, the static duckbill slides along the outer edge of the arc feeding plate. To prevent it from sliding out directly at the outer arc position, a block cover is placed at the lug of the hinge storage chute. The feeding accuracy of the static duckbill will directly affect the welding quality. Therefore, there are multiple through holes on the arc feeding plate and the connection plate, respectively, and the porous coordination ensures structural stability. The static duckbill and hinge feeding mechanism structure diagram is shown in Figure 13.

4.4. Design of Welding Fixture

As shown in Figure 14, the welding fixture is mainly composed of three parts: girdle clamping mechanism, hinge clamping mechanism, and static duckbill clamping mechanism. The girdle clamping device is positioned by a limit block and clamped by a girdle pusher. The girdle first slides down from the girdle storage chute to the girdle waiting area, and the girdle push plate sticks out. According to the four-point positioning principle, the transverse and longitudinal positioning and clamping of the girdle are completed.

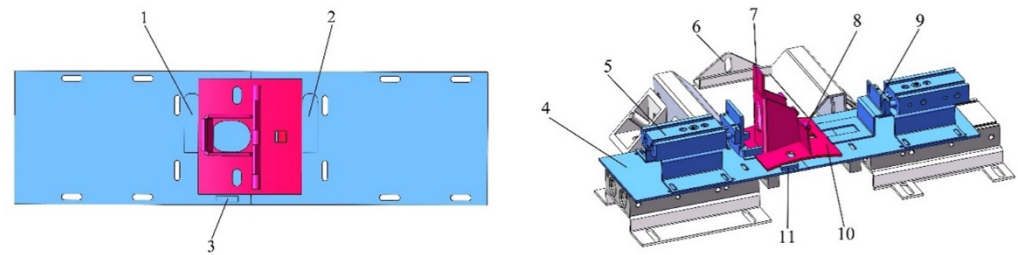


Figure 14. Structure diagram of welding fixture. 1. Limit block; 2. limit block; 3. limit block; 4. welding workbench; 5. static duckbill clamping device; 6. girdle push plate; 7. static duckbill; 8. hinge; 9. hinge clamping device; 10. girdle; 11. limit block.

The hinge clamping mechanism is composed of a guide bar and a hinge push plate. The guide bar is close to the side wall of the storage chute, symmetrically distributed on both sides, and plays a guiding and limiting role to the hinge. The guide bar is shown in the partially enlarged section of Figure 13. After the hinge is loaded onto the welding platform, the hinge is pushed out to complete the positioning of the hinge.

The static duckbill clamping mechanism is mainly composed of a cylinder and clamp push plate. The arc feeding plate supports and guides the static duckbill. After the static duckbill slides down to the welding workbench, the clamp push plate is pushed out to complete the horizontal and vertical positioning of the static duckbill.

The bottom of the welding workbench is composed of two welding bottom plates and two cylinders. The welding workbench can open and close under the action of the cylinder.

4.5. Welding Actuator

The schematic diagram of the welding actuator is shown in Figure 15. The welding actuator can move back and forth in a straight line along the X axis and Z axis. The stroke in the X axis direction is 100~150 mm, and the stroke in the Z axis direction is 150~200 mm. The double welding torch is symmetrically distributed on the welding torch bracket of the X axis linear slider. The movement of the X axis and Z axis is completed by the stepper motor electric drive synchronous belt module, and the movement speed is controlled by Siemens S7-1200PLC and the stepper motor driver. The Z axis selection has a brake stepper motor, which is locked when power fails, to prevent sliding.

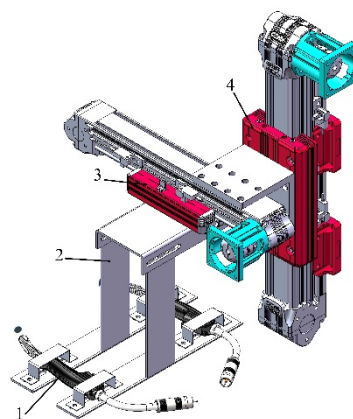


Figure 15. Welding actuator structure diagram. 1. Welding torch; 2. welding torch bracket; 3. X axis linear slider; 4. Z axis linear slider.

4.6. Control System Design

The cotton seeder duckbill welding robot controller is the Siemens S7-1200PLC. The communication between PLC and human-machine interaction (HMI) is Ethernet. PLC realizes manual and automatic control of the girdle, static duckbill, and hinge feeding operation. It also controls welding parameters, fixtures, welding actuators, and welding

platforms. HMI enables manual and automatic program switching of welding robots and monitors the working conditions of welding robots to ensure the safe and smooth operation of welding operations. The control system flow chart is shown in Figure 16.

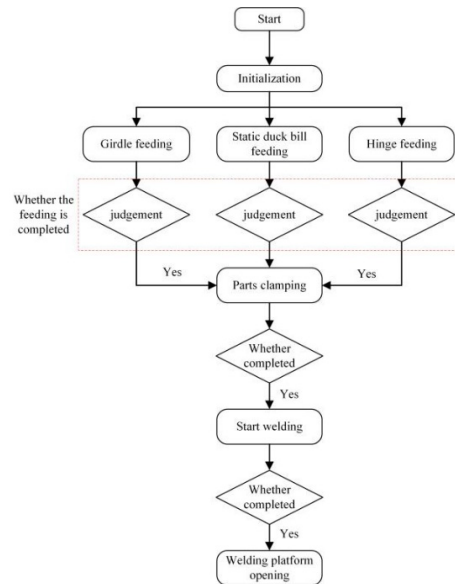


Figure 16. Control system flow chart.

5. Results and Discussion

5.1. Cotton Seeder Duckbill Welding Robot Test Results and Analysis

The welding wire used in the welding test is a 1.2 mm diameter solid wire (JQ-MG50-6; Tianjin Golden Bridge Welding Materials Group Co., Ltd., Tianjin, China), the protective gas is a mixture of CO₂ and argon gas, and the cotton planter duckbill welding robot was tested. The welding process parameters used in the test are shown in Table 3. The cotton seeder duckbill welding robot is shown in Figure 17.

Table 3. Welding process parameters.

Welding Current (A)	Welding Voltage (V)	Welding Speed (mm s)
38	26	10

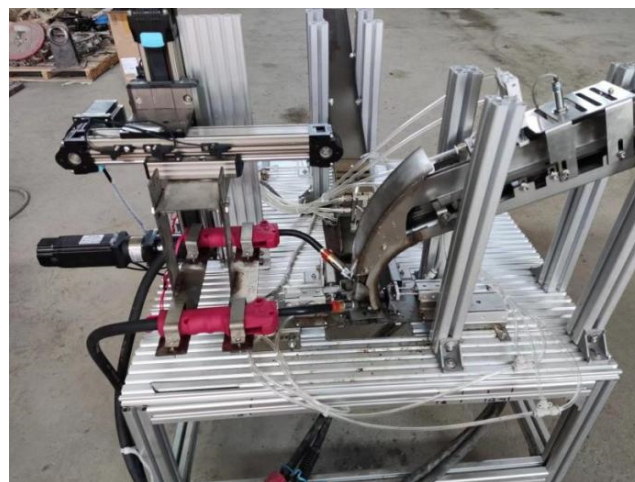


Figure 17. Cotton seeder duckbill welding robot.

The cotton seeder duckbill welding robot factory test photo is shown in Figure 18. The Human Machine Interface (HMI) of the cotton seeder duckbill welding robot is shown in Figure 19. According to the national standard DL/T 868-2004 welding procedure qualification procedure [32], the appearance of the weld after duck beak welding is analyzed. It can be seen from Figure 20 that there are no defects such as unmelted, porosity, and undercutting on the weld surface, and the welding quality is good. After testing, the welding efficiency of the cotton seeder duckbill welding robot is 6–7 times faster than that of the manual, and 600–800 duckbills can be welded per hour. The weld is well-formed. The welding pass rate is 85%, which can meet the needs of practical engineering. The development of the cotton seeder duckbill welding robot will greatly improve the welding efficiency of the duckbill parts and promote the large-scale and standardized production of the duckbill of the cotton seeder. The forming of welding parts is shown in Figure 20. The cotton seeder duckbill welding robot performance comparison is shown in Table 4.

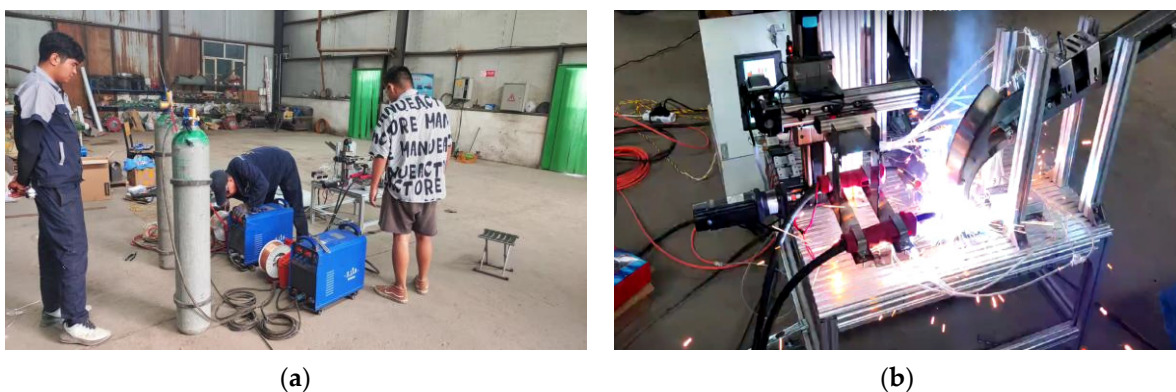


Figure 18. Factory test of cotton seeder duckbill welding robot. (a) Welding test site; (b) welding test in progress.

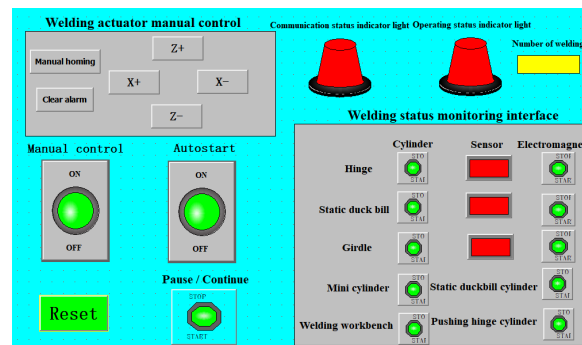


Figure 19. HMI.



Figure 20. Welding forming of duckbill parts.

Table 4. The cotton seeder duckbill welding robot performance comparison.

Assessment Indicators	Welding Method	Welding Duckbill Efficiency (Piece/h)	Welding Qualification Rate
Manual welding		100–130	99%
Semi-automatic duckbill welding equipment		200–300	100%
Cotton seeder duckbill welding robot		600–800	85%

5.2. Discussion

In this paper, a duckbill welding robot for cotton seeder is designed, including the mechanical structure and control system of the welding robot. The efficiency of a cotton seeder duckbill welding robot was greatly improved compared with manual work and semi-automatic welding robots, but there is still unqualified welding in the duckbill welding test. The main reason for this phenomenon is that there are some errors in the manufacturing and assembly of the parts of the duckbill welding robot for the cotton seeder. Mechanical vibration will occur during the operation, which will affect the accuracy of welding parts and the accuracy of welding gun welding. In the follow-up study, improving the welding robot parts manufacturing and assembly accuracy, and further optimizing the structure, will improve the welding robot welding qualification rate.

6. Conclusions

In this study, the characteristics of the duckbill parts were analyzed first, and then the welding process of the duckbill parts was simulated by Simufact Welding software. The whole process of welding was observed intuitively. At the same time, the deformation and stress changes of the weldment were compared and analyzed when the unilateral single welding torch and the bilateral symmetrical double welding torch, two welding forms, and two welding process parameters, were used. On this basis, a kind of cotton seeder duckbill welding robot was designed, and the welding test was carried out. The results show that the cotton seeder duckbill welding robot has high welding efficiency and good forming quality of welded parts. The design of the cotton seeder duckbill welding robot greatly improves the welding efficiency of the duckbill, which helps to solve the problems of low welding efficiency and unstable welding quality in manual welding and semi-automatic welding robots, and provides a strong guarantee for large-scale and standardized welding production of the duckbill.

Author Contributions: Writing—original draft preparation, Y.R.; writing—review and editing, W.G.; resources, X.W.; data curation, C.H.; visualization, L.W.; supervision, X.H. and J.X.; project administration, W.G. All authors have read and agreed to the published version of the manuscript.

Funding: This work was supported by the Bingtuan Science and Technology Program, grant number 2020CB034, and the Innovation research team project of Tarim University, grant number TDZKCX202103.

Institutional Review Board Statement: Not applicable.

Informed Consent Statement: Not applicable.

Data Availability Statement: The data presented in this study are available on request from the corresponding author.

Acknowledgments: Thanks for being grateful for the support of the Bingtuan Science and Technology Program (Grant No. 2020CB034), the Innovation research team project of Tarim University (Grant TDZKCX202103). The authors are grateful to anonymous reviewers for their comments.

Conflicts of Interest: The authors declare no conflict of interest.

References

1. Xie, Z.K.; Wang, Y.J.; Li, F.M. Effect of plastic mulching on soil water use and spring wheat yield in arid region of northwest China. *Agric. Water Manag.* **2005**, *75*, 71–83. [[CrossRef](#)]
2. Han, J.; Jia, Z.K.; Han, Q.F.; Zhang, J. Application of Mulching Materials of Rainfall Harvesting System for Improving Soil Water and Corn Growth in Northwest of China. *J. Integr. Agric.* **2013**, *12*, 1712–1721. [[CrossRef](#)]
3. Zhang, X.J.; Zhang, H.T.; Shi, Z.L.; Jin, W.; Cheng, Y.; Yu, Y.L. Design and experiments of seed pickup status monitoring system for cotton precision dibblers. *Trans. Chin. Soc. Agric. Eng.* **2022**, *38*, 9–19. [[CrossRef](#)]
4. Wang, Y.; Wei, M.; Dong, W.; Li, W.; He, J.; Han, C.; Jiang, Z. Design and Parameter Optimization of a Soil Mulching Device for an Ultra-Wide Film Seeder Based on the Discrete Element Method. *Processes* **2022**, *10*, 2115. [[CrossRef](#)]
5. Xiang, Y.; Kang, J.M.; Zhang, C.Y.; Peng, Q.J.; Zhang, N.N.; Wang, X.Y. Analysis and Optimization Test of the Peanut Seeding Process with an Air-Suction Roller Dibbler. *Agriculture* **2022**, *12*, 1942. [[CrossRef](#)]
6. Hrcek, S.; Brumerčik, F.; Smetanka, L.; Lukac, M.; Patin, B.; Glowacz, A. Global Sensitivity Analysis of Chosen Harmonic Drive Parameters Affecting Its Lost Motion. *Materials* **2021**, *14*, 5057. [[CrossRef](#)]
7. Majchrák, M.; Kohár, R.; Hrček, S.; Brumerčik, F. The Comparison of the Amount of Backlash of a Harmonic Gear System. *Teh. Vjesn.* **2021**, *28*, 771–778. [[CrossRef](#)]
8. Rheaume, F.-E.; Champlaud, H.; Liu, Z. Understanding and modelling the torsional stiffness of harmonic drives through finite-element method. *Proc. Inst. Mech. Eng. Part C J. Mech. Eng. Sci.* **2009**, *223*, 515–524. [[CrossRef](#)]
9. Subham, A.; Santonab, C.; Kanika, P.; Shankar, C. A Rough Multi-Attributive Border Approximation Area Comparison Approach for Arc Welding Robot Selection. *Jordan J. Mech. Ind. Eng.* **2021**, *15*, 169–180.
10. Stephen, C.; Joseph, O.; Stephen, Z. Zero Moment Control for Lead-Through Teach Programming and Process Monitoring of a Collaborative Welding Robot. *J. Mech. Robot.* **2021**, *13*, 031016. [[CrossRef](#)]
11. Shah, H.; Sulaiman, M.; Shukor, A.; Jamaluddin, M. A Review Paper on Vision Based Identification, Detection and Tracking of Weld Seams Path in Welding Robot Environment. *Mod. Appl. Sci.* **2016**, *10*, 83. [[CrossRef](#)]
12. Wang, X.W.; Xue, L.K.; Yan, Y.X.; Gu, X.S. Welding Robot Collision-Free Path Optimization. *Appl. Sci.* **2017**, *7*, 89. [[CrossRef](#)]
13. Yin, T.; Wang, J.P.; Zhao, H.; Zhou, L.; Xue, Z.H.; Wang, H.H. Research on Filling Strategy of Pipeline Multi-Layer Welding for Compound Narrow Gap Groove. *Materials* **2022**, *15*, 5967. [[CrossRef](#)] [[PubMed](#)]
14. ERSÖZ, S.; TÜRKER, A.; AKTEPE, A.; ATABAŞ, İ.; KOKOÇ, M. Design of a Tracking Welding Robot Automation System for Manufacturing of Steam and Heating Boilers. *Acad. Platf. J. Eng. Sci.* **2018**, *6*, 19–24. [[CrossRef](#)]
15. Ku, N.; Cha, H.; Lee, K.; Kim, J.; Kim, T.; Ha, S.; Lee, D. Development of a mobile welding robot for double-hull structures in shipbuilding. *J. Mar. Sci. Technol.* **2010**, *15*, 374–385. [[CrossRef](#)]
16. Mulligan, S.; Melton, J.; Lylynoja, A.; Herman, K. Autonomous welding of large steel fabrications. *Ind. Robot Int. J.* **2005**, *32*, 346–349. [[CrossRef](#)]
17. Jiang, Y.; Han, Q.Q.; Dai, Z.E.; Zhou, C.; Yu, J.F.; Hua, C.J. Structural design and kinematic analysis of a welding robot for liquefied natural gas membrane tank automatic welding. *Int. J. Adv. Manuf. Technol.* **2022**, *122*, 461–474. [[CrossRef](#)]
18. Yue, J.F.; Dong, X.T.; Guo, R.; Liu, W.J.; Li, L.Y. Numerical simulation of equivalent heat source temperature field of asymmetrical fillet root welds. *Int. J. Heat Mass Transf.* **2019**, *130*, 42–49. [[CrossRef](#)]
19. Zhao, H.Q.; Zhang, Q.Y.; Niu, Y.X.; Du, S.Z.; Lu, J.H.; Zhang, H.F.; Wang, J.C. Influence of triangle reinforcement plate stiffeners on welding distortion mitigation of fillet welded structure for lightweight fabrication. *Ocean Eng.* **2020**, *213*, 107650. [[CrossRef](#)]
20. Maarten, R.; Richard, P.; Henk, S.; Johan, M. A combined experimental and numerical examination of welding residual stresses. *J. Mater. Process. Technol.* **2017**, *261*, 98–106. [[CrossRef](#)]
21. Ahn, J.; He, E.; Chen, L.; Pirling, T.; Dear, J.P.; Davies, C.M. Determination of residual stresses in fibre laser welded AA2024-T3 T-joints by numerical simulation and neutron diffraction. *Mater. Sci. Eng. A* **2018**, *712*, 685–703. [[CrossRef](#)]
22. Li, Z.; Peng, W.X.; Chen, Y.Z.; Liu, W.H.; Zhang, H.Q. Simulation and experimental analysis of Al/Ti plate magnetic pulse welding based on multi-seams coil. *J. Manuf. Process.* **2022**, *83*, 290–299. [[CrossRef](#)]
23. Lu, B.; Ni, X.D.; Li, S.F.; Li, K.Z.; Qi, Q.Z. Simulation and Experimental Study of a Split High-Speed Precision Seeding System. *Agriculture* **2022**, *12*, 1037. [[CrossRef](#)]
24. Bai, S.H.; Yuan, Y.W.; Niu, K.; Shi, Z.L.; Zhou, L.M.; Zhao, B.; Wei, L.G.; Liu, L.J.; Zheng, Y.K.; An, S.; et al. Design and Experiment of a Sowing Quality Monitoring System of Cotton Precision Hill-Drop Planters. *Agriculture* **2022**, *12*, 1117. [[CrossRef](#)]
25. Mehran, J.; Antti, A.; Joseph, A.; Timo, B. Numerical and experimental investigations on the welding residual stresses and distortions of the short fillet welds in high strength steel plates. *Eng. Struct.* **2022**, *260*, 114269. [[CrossRef](#)]
26. Go, B.S.; Oh, K.H.; Kwon, S.; Bang, H.S. Reduction Characteristics of Welding Deformation According to Cooling Distance in Heat Sink Welding. *Int. J. Precis. Eng. Manuf.* **2022**, *23*, 1229–1236. [[CrossRef](#)]
27. Ikushima, K.; Maeda, S.; Shibahara, M. Ultra Large-Scale Nonlinear FE Analysis of Welding Mechanics. *Int. Conf. Comput. Exp. Eng. Sci.* **2019**, *22*, 175. [[CrossRef](#)]
28. Farias, R.M.; Teixeira, P.R.F.; Vilarinho, L.O. Variable profile heat source models for numerical simulations of arc welding processes. *Int. J. Therm. Sci.* **2022**, *179*, 107593. [[CrossRef](#)]
29. Farias, R.M.; Teixeira, P.R.F.; Vilarinho, L.O. An efficient computational approach for heat source optimization in numerical simulations of arc welding processes. *J. Constr. Steel Res.* **2021**, *176*, 106382. [[CrossRef](#)]

30. Goldak, J.; Chakravarti, A.; Bibby, M. A new finite element model for welding heat sources. *Metall. Mater. Trans. B* **1984**, *15*, 299–305. [[CrossRef](#)]
31. Yan, X.H.; Chen, G.Q.; Xu, H.L.; Yan, Z.Y.; Li, P. Welding Quality Control of Control Rod of Lawn Mower Cutter Plate Based on Simufact. *J. Netshape Form. Eng.* **2022**, *14*, 46–50.
32. *DL/T 868-2004*; The Code of Welding Procedure Qualification [S]. Power Standards: China, 2004.

Disclaimer/Publisher's Note: The statements, opinions and data contained in all publications are solely those of the individual author(s) and contributor(s) and not of MDPI and/or the editor(s). MDPI and/or the editor(s) disclaim responsibility for any injury to people or property resulting from any ideas, methods, instructions or products referred to in the content.